Characteristics of Summer Airflow over the Antarctic Peninsula in Response to Recent Strengthening of Westerly Circumpolar Winds

ANDREW ORR,*,** GARETH J. MARSHALL,+ JULIAN C. R. HUNT,* JOEL SOMMERIA,#
CHANG-GUI WANG,@ NICOLE P. M. VAN LIPZIG,& DOUG CRESSWELL,* AND JOHN C. KING+

*Centre for Polar Observation and Modelling, University College London, London, United Kingdom
+British Antarctic Survey, Natural Environment Research Council, Cambridge, United Kingdom
#LEGI/Coriolis, Grenoble, France
@Department of Meteorology, University of Reading, Reading, United Kingdom
&Physical and Regional Geography Research Group, K. U. Leuven, Heverlee, Belgium

(Manuscript received 17 April 2007, in final form 2 August 2007)

ABSTRACT

Summer near-surface temperatures over the northeast coast of the Antarctic Peninsula have increased by more than 2°C over the past 40 years, a temperature increase 3 times greater than that on the northwest coast. Recent analysis has shown a strong correlation between this striking warming trend and significant change in the summer Southern Hemisphere annular mode (SAM), which has resulted in greatly increased summer westerlies across the northern peninsula. It has been proposed that the strengthening westerlies have resulted in increased vertical deflection of relatively warm maritime air over the northern peninsula, contributing significantly to the observed warming and the recent collapse of northern sections of the Larsen Ice Shelf. In this study, laboratory and numerical modeling of airflow incident to the peninsula are employed to further understand this mechanism. It is shown that the effect of the strengthening westerlies has led to a distinct transition from a "blocked" regime to a "flow-over" regime, that is, confirmation of the proposed warming mechanism. The blocked regime is dominated by flow stagnation upstream (i.e., little vertical deflection) and consequent lateral deflection of flow along the western side of the peninsula. The flow-over regime is dominated by vertical deflection of mid/upper-level air over the peninsula, with strong downslope winds following closely to the leeward slope transporting this air (which warms adiabatically as it descends) to the near-surface of the northeast peninsula. The strong rotation typical of high latitudes considerably increases the flow over the peninsula, particularly strengthening it over the southern side (verified by aircraft measurements), suggesting that the warming trend is not solely confined to the northeast. Globally, flow regime transitions such as this may be responsible for other local climate variations.

1. Introduction

The Antarctic Peninsula stretches approximately northward from ~73° to 62°S (around 1500 km in length) with its west coast comparatively mild compared to the east coast (see Fig. 1). This difference in climate is maintained by the effect on the atmosphere of the high mountains of the peninsula (King et al. 2003). These have a maximum height of over 2000 m and a breadth of around 200 km and act as a formidable obstacle for the strong westerly winds that dominate the mean atmospheric circulation around Antarctica.

The peninsula region has undergone a remarkable warming trend since the mid–twentieth century, characterized by considerable interannual variability. Previously, most attention has been given to the warming trend experienced by the relatively accessible western Antarctic Peninsula, where annual average near-surface temperatures have increased by around 3°C over the past 50 years (e.g., King 1994; King and Harangozo 1998; Vaughan et al. 2001). By contrast, the east coast of the peninsula is less accessible and, hence, has considerably fewer and generally shorter continuous climate records than does the west coast. However, recent data from the northeast peninsula have demon-

** Current affiliation: ECMWF, Reading, United Kingdom.

Corresponding author address: Dr. Andrew Orr, ECMWF, Shinfield Rd., Reading RG2 9AX, United Kingdom.
E-mail: andrew.orr@ecmwf.int

DOI: 10.1175/2007JAS2498.1

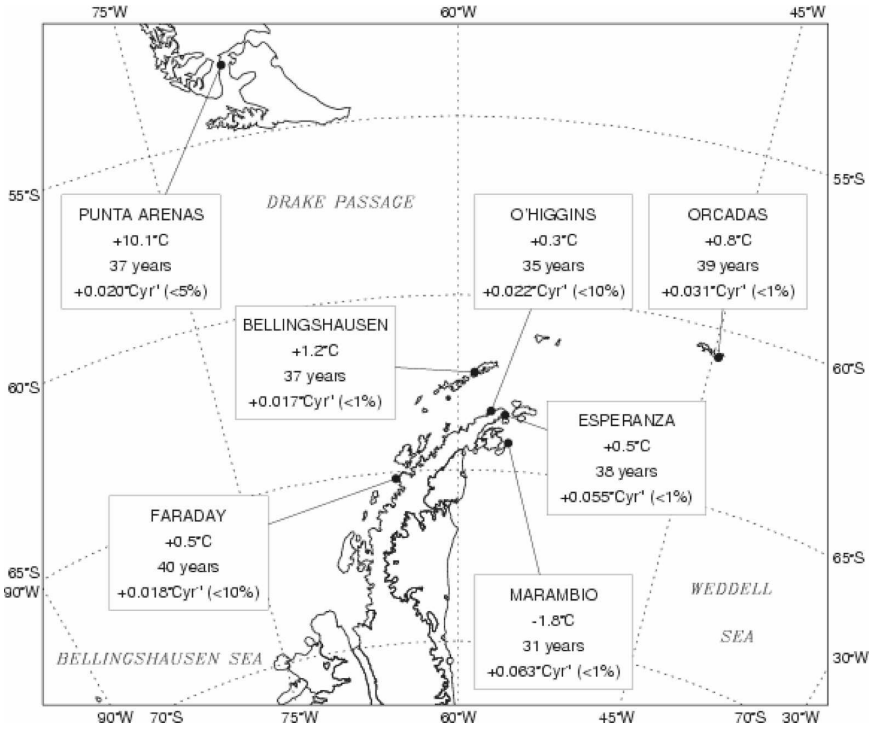

FIG. 1. Map of the northern Antarctic Peninsula and southern South America region showing summer near-surface temperature trends at research stations (not all of which are mentioned in the text) for the period 1965–2004. The mean summer temperature (°C) for this period is shown. The length of the observation record is given in years. The mean summer temperature trend (and the statistical significance) is given in °C yr^{-1}. The Larsen Ice Shelf is situated on the eastern side of the peninsula.

strated a significant summer warming trend, comparable and in phase with the overall peninsula warming (see Fig. 1). Over the past 40 years, summer near-surface temperatures at Esperanza (see Fig. 1) have increased by around 2°C at near-surface level, three times faster than observed over the northwest peninsula (King et al. 2003). Here the southward migration of the 0°C isotherm amplifies any warming and is thought to be responsible for the recent collapse of northern sections of the Larsen Ice Shelf (see Fig. 1; Marshall et al. 2006; Vaughan et al. 2003).

Coincident with these recent warming trends has been a marked strengthening of the circumpolar westerly flow (Marshall 2002). This result is consistent with the trend since the mid-1960s toward the positive phase of the Southern Hemisphere annular mode (SAM) (Marshall 2003). This index describes an annular structure in variability with synchronous pressure anomalies of opposite sign above Antarctica and the southern midlatitudes. Kwok and Comiso (2002), Thompson and Solomon (2002), and Van den Broeke and Van Lipzig (2003) have shown the influence of the more positive phase SAM on the observed warming patterns over the peninsula. Orr et al. (2004) showed that the strengthening westerlies led to increased blocking of low-level air upstream of the peninsula, resulting in stronger northerlies transporting greater amounts of relatively warm air along its western side, which contributed to the warming trend here. The significant role that this mechanism had in autumn (and annual) warming of the western side was confirmed by Marshall et al. (2006). However, the strengthening is especially marked during summer, with observations at Bellingshausen, situated at the northern tip of the peninsula (see Fig. 1), showing that during this season for the period 1969 to 1998 the mean westerly flow at a height of 850 hPa increased from around 7 to 12.5 m s^{-1} (Marshall et al. 2006).

To further understand this trend, Marshall et al. (2006) produced a climatology of summers with positive and negative SAM indexes using European Centre for Medium-Range Weather Forecasts (ECMWF) Re-Analysis (ERA-40) fields. These showed that during this season the positive trend in the SAM led to *increased flow over* the peninsula, advecting relatively warm air to the northeast coast and increasing the near-surface temperature over the northeast peninsula (i.e.,

at Esperanza). Additionally, the strengthening westerlies means weaker synoptic easterlies, resulting in reduced blocking and southerlies along the eastern side and decreasing the transport of air from cold southerly latitudes along the east coast (Orr et al. 2004). Marshall et al. further demonstrated using observations that for the period 1965–2000 the positive trend in the SAM contributed around 1.3°C warming to the northeast peninsula during summer, compared to around 0.4°C warming to the northwest peninsula region. Both Thompson et al. (2000) and Marshall et al. (2004) showed that the positive trend in the SAM is most pronounced in the summer season.

The contrasting sea ice regimes on either side of the peninsula strengthen the seasonal nature of the warming trend. In most years the sea ice coverage on the western side of the peninsula during summer has retreated back to the southern parts of the Bellingshausen Sea. By contrast, with the exception of the northeast part, the eastern side usually remains icebound during summer (King et al. 2003). On the western side the lack of sea ice results in the approaching moist maritime air masses being relatively warm and, hence, less dense, thus better able to rise over the peninsula. Summer temperatures here are significantly warmer than the colder continental air generally found over the Weddell Sea, east of the peninsula, so an increase in advection over the peninsula will result in increasing temperatures here. Moreover, the air mass cools as it is lifted up, causing condensation and the formation of clouds (Van Lipzig et al. 2008) and warming of the air by latent heat release. If the air is lifted over the barrier, due to it being denser than its surroundings it descends the leeward slope under the influence of gravity. Warming and drying of this downslope wind occurs by adiabatic compression heating. The air mass can typically "overshoot" its equilibrium level and descend to the lower altitudes at the base of the lee slope. These high-speed, turbulent winds are able to penetrate or displace any existing cold, moist air mass, thus enhancing the temperature increase and the humidity decrease at near surface (Beran 1967). This is particularly possible over the northeast peninsula during summer as the lack of sea ice means that the overlying atmosphere will be comparatively weakly stratified.

Extensive work has been done on studying the flow characteristics over mountains such as the Pyrenees (e.g., Georgelin and Richard 1996), the Rocky Mountains (e.g., Boyer and Chen 1987), and Greenland (e.g., Orr et al. 2005). Although Baines and Fraedrich (1989) presented a laboratory study on the effects of topography on the mean flow pattern above Antarctica, there have not been any detailed studies concentrating specifically on the peninsula region. Note that the peninsula differs fundamentally from these other mountain ranges by having one side attached to the high mountain plateau of Western Antarctica and the Transantarctic mountains (~2000 m), which effectively blocks low-level flow from passing around the peninsula's southern end. This study attempts to redress this deficit by considering the results of a laboratory model of simple idealized flow incident to a "cape." Further detailed understanding is provided by numerical mesoscale modeling of selected cases of westerly flows interacting with the peninsula. Of particular importance will be to understand the sensitivity of the response to strengthening westerly circumpolar flow and its role in driving the large summer warming observed over its northeast side.

The structure of the paper is as follows: section 2 is a review of the nature of nonrotating and rotating stratified flow over mountains and introduces the relevant nondimensional numbers; the laboratory and numerical modeling are described in sections 3 and 4, respectively; and a discussion is given in section 5.

2. Review of stratified flow regimes over mountains

The nature of stratified airflow over mountains is defined by the nondimensional mountain height $\hat{h} = Nh/U$, where U is the speed of the oncoming flow, h is the mountain height, and N is the Brunt–Väisälä frequency (Baines 1995). Airflow over *sufficiently high* orography is characterized by large $\hat{h}$ (i.e., $\hat{h} > 1$) and by highly nonlinear phenomena such as flow stagnation upstream of the windward slope or some distance above the leeward slope, wave breaking, downslope winds, and lee vortices, as reviewed by Smith (1989). Airflow over *sufficiently low* orography is characterized by small $\hat{h}$ (i.e., $\hat{h} < 1$) and linear phenomena such as streamlines to the side passing smoothly around the hill, while the center streamline passes over the top of the hill in the form of a smooth mountain wave (Smith 1989).

Flow stagnation upstream of the windward slope is called blocking, which is associated with subcritical internal waves of mode n and velocity $Nd/n\pi > U$ propagating against the flow; that is, $F < 1$ where the Froude number $F = U/(Nd/\pi)$ and d is the fluid depth. For $F > 1$ the flow is supercritical and no modes may propagate upstream (Baines 1995). Additionally, blocking is associated with a stagnation point from where flow splitting occurs, with streamlines diverging and descending in approximately horizontal planes around the mountain

(Pierrehumbert and Wyman 1985). This has been reproduced in field experiments (e.g., Vosper et al. 1999) and simulated experimentally (e.g., Baines and Smith 1993). As the flow separates on the lee side, large recirculating eddies are formed (e.g., Ding and Street 2003). Baines (1979) showed that all flow incident to a two-dimensional barrier was blocked if $\hat{h} \approx 2$.

For a three-dimensional barrier, Baines (1979) observed blocked flow below a certain height z_d ($<h$) passing around the barrier with flow above this dividing streamline height being vertically deflected over the barrier (i.e., flow-over) and with strong downslope winds following closely to the leeward slope. Hunt and Snyder (1980) showed for an isolated hill $z_d = h(1 - \alpha/\hat{h})$, with α a constant of order 1. As $\hat{h}$ increases, the vertical extent of the blocked region increases, decreasing the amount of flow over the mountain (Baines and Smith 1993). Whether air flows around or over an obstacle is also dependent on the mountain shape (e.g., Baines and Hoinka 1985), the gap width around the obstacle (Baines 1979), and its aspect ratio $R = B/D$ (e.g., Baines and Smith 1993), where B and D are the obstacle length and breadth respectively. Hunt and Snyder (1980) showed that for a circular hill (i.e., $R = 1$) $\alpha \approx 1$. If the mountain is a ridge orientated perpendicular to the flow, that is, $R \gg 1$, it becomes easier for flow to pass over the obstacle. Ólafsson and Bougeault (1996) showed that $\alpha \approx 1.2$ for a mountain ridge with $R = 5$.

Flow stagnation above the leeward slope is associated with streamlines becoming steeply sloping, and overturning with local wave breaking (Hunt et al. 1997) severely affecting the flow field, not least in the possibility of producing much stronger downslope winds in the lee (Lilly 1978). For both a circular shaped hill (Smith and Grønås 1993) and mountain ridge (Ólafsson and Bougeault 1996), stagnation first occurs above the leeward slope. Moreover, for sufficiently large $\hat{h}$, wave breaking over a mountain ridge ceases over its axis of symmetry and is, instead, limited to narrow regions on the flanks (Ólafsson and Bougeault 1996).

Moreover, flow behavior is also dependent on the effects of the earth's rotation, that is, the Coriolis force, characterized by the Rossby number $\mathrm{Ro} = 2U/fD$ (where f is the Coriolis parameter). The Coriolis force is proportional to velocity and in the Southern Hemisphere acts to the left. The effect of strong Coriolis force (small Ro) and sufficiently large $\hat{h}$ is that the upstream extent of flow stagnation is limited to a distance of the order of the Rossby deformation radius $L_R = Nh/f$. Rather than the blocked flow diverting either side of the mountain (as in the nonrotating case), it is diverted more to the right in the Southern Hemisphere (looking downstream) due to the Coriolis force decreasing in response to the flow deceleration. The diverted or split flow accelerates and low-level winds (or "barrier jets") form parallel to the ridge line (Pierrehumbert and Wyman 1985). As the air goes around the ends of the mountain, wind speeds are greater on the right-hand side than the left-hand side. The accelerating effect of rotation delays the onset of blocking, making it easier for flow to rise over the obstacle (Ólafsson and Bougeault 1997). The asymmetrical effect of the Coriolis force increases with the aspect ratio. Ólafsson (2000) showed, for an elongated mountain with $R = 5$, decreasing Ro from 2.5 to 0.5 increased the value of $\hat{h}$, which determined the onset of blocking from between 1.4 and 2.5 to greater than 2.7. Low-level jets occur downstream of the mountain at either side of the wake (Hunt et al. 2001). For very large mountains where $B \gg L_R$, sufficiently large deflections can occur such that the mean wake structure changes from two symmetrical separated eddies to a flow that encircles the mountain (Orr et al. 2005).

Additionally, for an elongated mountain horizontal convergence and upward motion increases the amount of diverted air flowing over its right-hand side (Orr et al. 2005). Here, the steepness of the sloping streamlines encourages greater wave breaking (Ólafsson and Bougeault 1997). Similarly, Hunt et al. (2001) showed upward deflection of isopycnals over the mountains right-hand side (with downward deflection over the left-hand side), resulting in accumulation of low-level dense air above the right-hand leeward slope.

Relevant Antarctic Peninsula parameter space

Based on the trend of strengthening 850-hPa westerly velocity observed at Bellingshausen (and taking $h \sim 1500$ m as representative of the height of the *northern* section of the peninsula and $N \sim 0.01\ \mathrm{s}^{-1}$ as typical of stable Antarctic airflow), during 1969 to 1998 the characteristic summer nondimensional mountain height of the northern section of the Antarctic Peninsula decreased from $\hat{h}_{\mathrm{weak}} \sim 2.14$ to $\hat{h}_{\mathrm{strong}} \sim 1.20$. Here $F_{\mathrm{weak}} \sim 0.24$ and $F_{\mathrm{strong}} \sim 0.44$ (taking the summer troposphere height as around 9000 m). Taking $f \sim 1.3 \times 10^{-4}\ \mathrm{s}^{-1}$ as representative of the high latitude of the peninsula and $D \sim 200$ km gives $\mathrm{Ro}_{\mathrm{weak}} \sim 0.53$, $\mathrm{Ro}_{\mathrm{strong}} \sim 0.96$, and $L_R \sim 150$ km. Taking $B \sim 1500$ km gives $R \sim 7.5$ and $B/L_R \sim 10$. Wind speeds based on the ERA-40 reanalysis climatology of summers with a positive SAM phase shift (SAM+) and negative SAM phase shift (SAM−) by Marshall et al. (2006) are perhaps more representative of the flow incident to the actual northern section of the peninsula (i.e., farther south than Bellings-

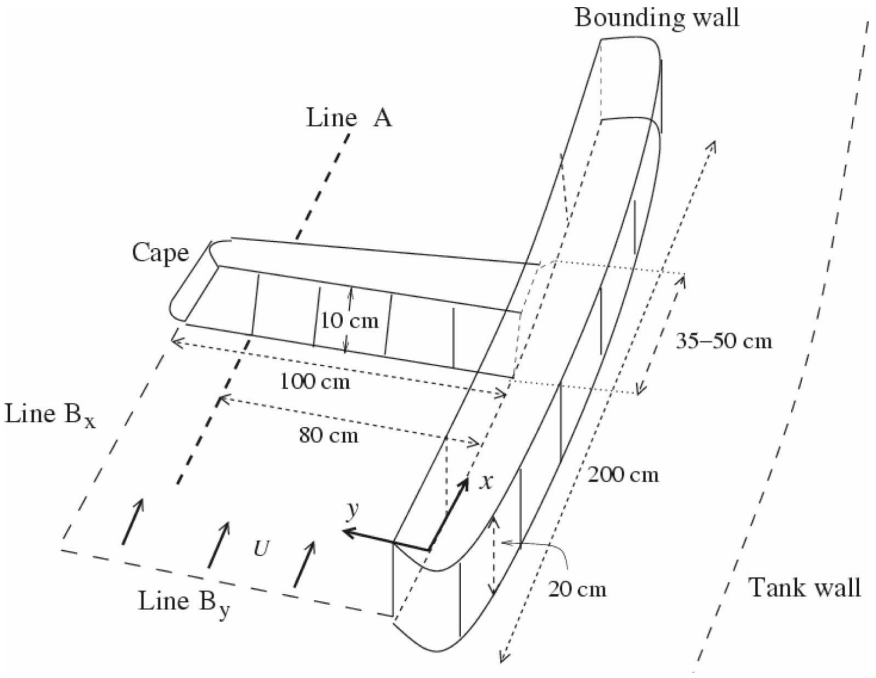

FIG. 2. Schematic illustration of the experimental setup (not drawn to scale) presented in a frame coordinate equivalent to the experiment being performed in the Southern Hemisphere. The Antarctic Peninsula is simulated by a "cape" orientated perpendicular to an anticlockwise or westerly flow. Note the directions x and y orientated parallel and perpendicular to the upstream flow direction; $y = 0.8B$ is defined at the position of a vertical cross section perpendicular to the cape, and labeled as line A (see Figs. 3 and 6).

hausen). Here the upstream velocity at 850-hPa height showed $U_{\mathrm{SAM}-} \approx 5\ \mathrm{m\ s^{-1}}$ and $U_{\mathrm{SAM}+} \approx 8\ \mathrm{m\ s^{-1}}$, significantly slower than those observed at Bellingshausen, giving $\hat{h}_{\mathrm{SAM}-} \sim 3.00$ ($>\hat{h}_{\mathrm{weak}}$) and $\hat{h}_{\mathrm{SAM}+} \sim 1.88$ ($>\hat{h}_{\mathrm{strong}}$), with $F_{\mathrm{SAM}-} \sim 0.17$ and $F_{\mathrm{SAM}+} \sim 0.28$, and $\mathrm{Ro}_{\mathrm{SAM}-} \sim 0.38$ ($<\mathrm{Ro}_{\mathrm{weak}}$) and $\mathrm{Ro}_{\mathrm{SAM}+} \sim 0.62$ ($<\mathrm{Ro}_{\mathrm{strong}}$). For SAM+ a "flow-over" regime dominated; that is, the high aspect ratio and low Rossby number of the Antarctic Peninsula increases the value of $\hat{h}$ [$\hat{h}_{\mathrm{SAM}+}$ (and $\hat{h}_{\mathrm{strong}}$) > 1] for which flow travels easily over the obstacle. For SAM− a "blocked" flow regime dominated.

3. A laboratory model of simple idealized flow incident to a cape

A laboratory experiment modeling flow over the peninsula and its sensitivity to the nondimensional mountain height was undertaken. Additional experiments were carried out to determine the sensitivity of the flow regime to the Rossby number. The experiments were performed in the large rotating circular tank (13 m in diameter) on the Coriolis turntable, Grenoble, France. The peninsula was represented by a simple "cape" consisting of a radial barrier of height $h = 10$ cm and length $B = 100$ cm (i.e., in the crosswind or y direction). One end of the cape with width $D = 50$ cm (i.e., in the along-wind or x direction) abuts onto a bounding wall (parallel to the mean flow and mirroring the effect of the Transantarctic Mountains) of height 20 cm. The other end tapers to a width $D = 35$ cm at the cape's tip, which is also rounded. This obstacle was placed on the tank floor, ~1 m from the tank edge, and orientated so that the incident flow was perpendicular to it. See Fig. 2.

The tank was slowly filled while rotating with a saline aqueous solution providing a linear stratification, obtained by a computer-controlled pumping from two tanks containing brine and pure water, to a depth $d = 60$ cm, giving a constant density gradient and $N \approx 0.6\ \mathrm{s^{-1}}$. The ratio $h/d = 0.17$ is approximately equal to the atmospheric value (taking $d \sim 9000$ m and $h \sim 1500$ m). During this time the turntable was "spun up" from rest to a period $T = 125$ s, rotating in an anticlockwise direction. Once filled it was left for a period of a few hours to ensure the fluid had reached a steady state. Fluid motion was generated by impulsively decreasing the period to $T = 100$ s, producing a clockwise flow with

$f = 4\pi/T = 0.13\ \mathrm{s}^{-1}$ and an initial velocity of $U \approx 5$ cm s^{-1} relative to the cape (Boyer and Davies 2000), which decayed within an hour to around 1 cm s^{-1}. Here U is defined as the velocity in the zonal or x direction, and V is defined as the velocity in the meridional or y direction. The fluid motion induced mixing at low levels to the lee of the cape. This impaired the uniform stratification and generated an inversion near the tank floor varying in height between $0.3h$ and $0.7h$ [this height is considerably greater than the inversion height typical of the peninsula (King and Turner 1997)].

The large value of the Coriolis parameter simulates the low Rossby number regime typical of the peninsula. As the experiments were performed in the Northern Hemisphere, the clockwise flow relative to the cape is equivalent to an anticlockwise or westerly flow in the Southern Hemisphere. Figure 2 and the experimental results hereafter are presented in this "Southern Hemisphere" frame coordinate.

The technique for flow visualization involved placing a large number of neutrally buoyant polystyrene particles in the fluid and illuminating the tank with a thin horizontal beam of light produced by a laser (i.e., a light sheet) at some particular level. The flow field at each level was recorded by a camera fixed above the cape, taking bursts of four images at each level. This procedure was repeated five times for each observation. Pairs of images from each burst were analyzed using Correlation Imaging Velocimetry (CIV) to determine the velocity field (Fincham and Delerce 2000). The five velocity fields for each level were averaged to give a single result (with an uncertainty estimated to be less than $\pm 5\%$).

Due to refraction associated with the density gradient of the fluid, the laser sheet sloped downward in the direction of the bounding wall. Initial calibration showed that the height of the lowest vertical level of the light sheet was 0.4–$0.5h$ near the tip of the cape and 0.1–$0.2h$ at the bounding wall. Moreover, owing to the low-level mixing the vertical height of the lower levels changed through the experiment. However, heights at the tip of the cape could be reliably estimated by visually determining the level at which the light sheet intersected the cape (with an uncertainty of around $\pm h/40$).

a. Description of blocked and flow-over regimes

Here U_0 is defined as the zonal velocity at a height h (i.e., level with the summit of the cape), upstream of the tip of the cape. Two flow fields were investigated with U_0 measured as 2.1 and 3.4 cm s^{-1}, giving $\hat{h} \approx 2.86$ (i.e., representative of the $\hat{h}_{\mathrm{SAM}-}$ flow regime) and $\hat{h} \approx 1.77$ (i.e., representative of the $\hat{h}_{\mathrm{SAM}+}$ flow regime), respectively. The inversion height downstream of the cape tip was around $0.7h$ and $0.3h$, respectively. Figure 3 shows normalized zonal and meridional velocities in a vertical cross section perpendicular to the cape and passing through line A in Fig. 2 (i.e., through the "northern" portion of the cape at $y = 0.8B$ with $y = 0$ at the bounding wall and $y = B$ at the tip of the cape). Data are only available from a height of around $z \approx 0.4h$. Here $D \sim 40$ cm (based on the width at the surface), giving Rossby numbers of 0.81 and 1.31, respectively (i.e., approximately representative of the Rossby numbers characteristic of the peninsula). Figure 4 shows the normalized horizontal and vertical velocity fields at the lowest vertical level examined. Here $L_R \sim 50$ cm; that is, $B/L_R \sim 2$. Note: the horizontal and vertical velocities are normalized by U_0 and $U_0 h/D$, respectively.

Froude numbers are 0.18 and 0.30 (associated with internal wave modes 5 and 3, respectively), so either typical ($F_{\mathrm{SAM}-} \sim 0.17$ and $F_{\mathrm{SAM}+} \sim 0.28$) or smaller ($F_{\mathrm{weak}} \sim 0.24$ and $F_{\mathrm{strong}} \sim 0.44$; associated with wave modes 4 and 2) than those observed. This suggests that the upstream behavior of the observed flow is generally well captured.

1) BLOCKED REGIME

Figure 3a shows the vertical cross section of the flow incident to the cape characterized by $\hat{h} \approx 2.86$ and $\mathrm{Ro} \approx 0.81$. The dividing streamline height is estimated as $z_d \approx 0.7h$ (giving $\alpha \approx 0.86$), though this is approximate due to the scarcity of measurements in this region. For $z < z_d$ the upstream flow within a distance of the order L_R of the cape slows; that is, a blocked regime dominates. As the cape is approached the flow rises slightly and is deflected to the left (looking downstream) with a meridional velocity of around 0.1–$0.2U_0$. The slight velocity speed-up that occurs aloft of the cape, due to convergence, confirms that a limited amount of upstream flow is being deflected over the obstacle. The speed-up aloft of the cape increases the Coriolis force, which deflects the accelerating flow strongly to the left with a meridional velocity approaching $0.4U_0$. The flow descends over the cape, continuing down the leeward slope for a considerable distance. Downwind and below the height of the cape the relatively slow zonal flow shows a slight lee wave with a wavelength of the order L_R. The accompanying meridional flow is deflected to the left with a velocity of 0.3–$0.4U_0$. At upper levels above the leeward slope (i.e., $z \approx 2h$), although the zonal flow is largely unaffected by the cape, there is still a significant deflection to the left.

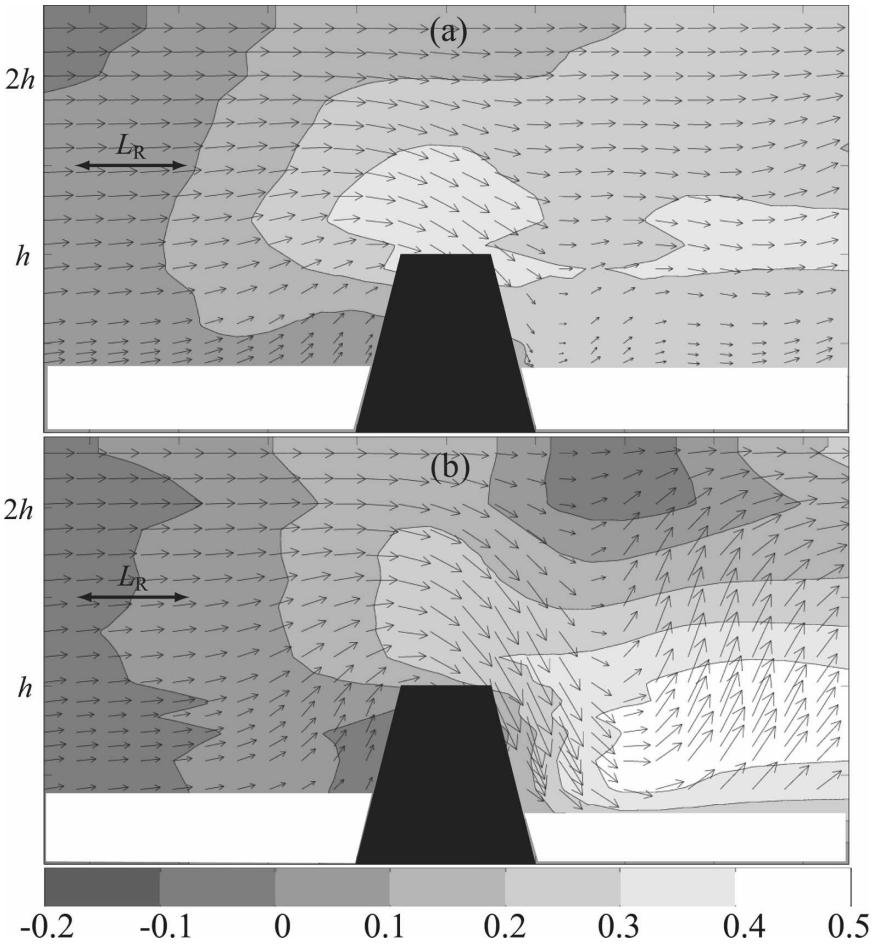

FIG. 3. Vertical cross section of normalized zonal (vectors) and meridional (shading) velocity of simulated westerly flow (left to right) with strong rotation incident to a cape in the Southern Hemisphere, passing through line A of Fig. 2 (i.e., through the "northern" portion of the cape at $y = 0.8B$): (a) $\hat{h} \approx 2.86$ and Ro ≈ 0.81 and (b) $\hat{h} \approx 1.77$ and Ro ≈ 1.31. The masked areas depict the cape cross section. Data are restricted to above the level of $0.4h$. The horizontal and vertical axes are drawn at different scales. Negative meridional values indicate northerly flow and are denoted by white dotted contours. The scale labeled L_R denotes the Rossby deformation radius.

Figure 4a shows that at low level ($z \approx 0.4h$) the upstream flow is blocked and divides around the cape. A stagnation point in the flow occurs at $y \approx 0.7B$. To the left of this (looking downwind) the flow is deflected toward the tip of the cape, consistent with Fig. 3a. As it passes around the tip it forms a "detached jet" downstream at an angle of around 45° to the x axis with velocities around twice those of upstream. To the right of this the flow is deflected toward the bottom of the cape by the Coriolis force, forming a barrier jet. Here the vertical velocity is small, ~ 0–$0.5U_0h/D$. Downstream of the cape and immediately parallel to the leeward slope the vertical velocity is approximately $-U_0h/D$, consistent with the evidence from Fig. 3a that the downslope flow is stronger than the corresponding upslope flow. Farther downstream alternating regions of progressively weaker ascending and descending flow are evident, consistent with the lee wave shown in Fig. 3a. A "lee jet" originating mainly from the middle section of the cape develops downstream. This is deflected strongly to the left, traveling in the same direction as the detached jet. Centered on this jet are regions where vertical velocities are largest. The jet decays downstream over a distance of around $2L_R$.

2) FLOW-OVER REGIME

Figure 3b shows the vertical cross section of the flow characterized by $\hat{h} \approx 1.77$ and Ro ≈ 1.31. Here $z_d \approx$

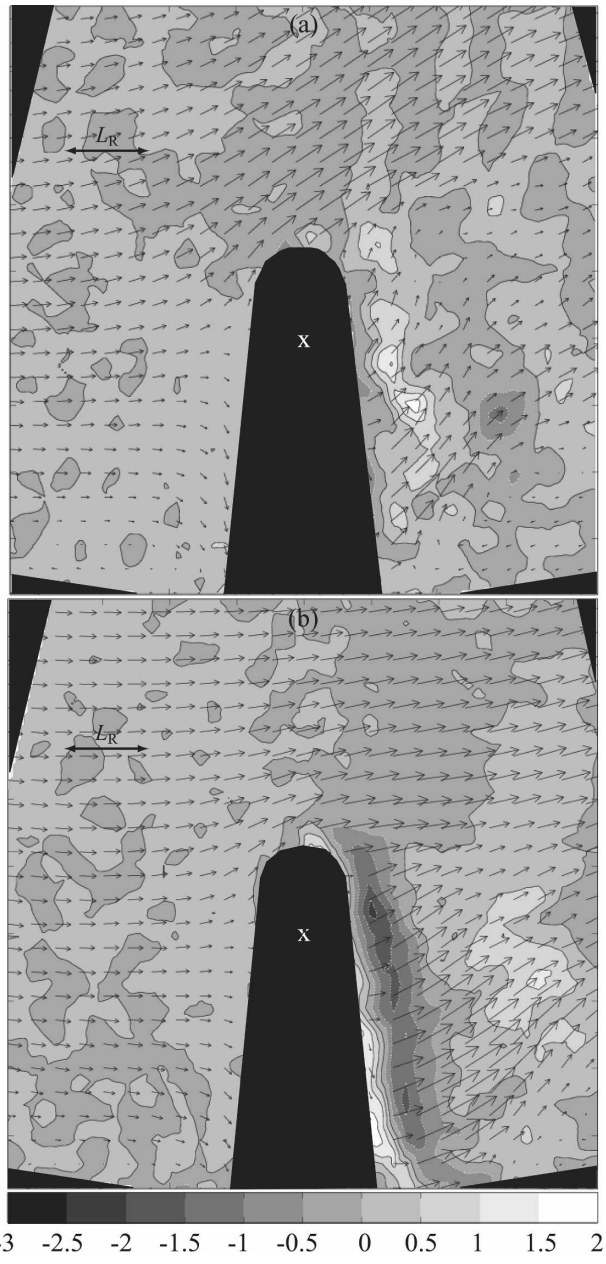

FIG. 4. Normalized horizontal (vectors) and vertical (shading) velocity at a height $z \approx 0.4h$ of simulated westerly flow (left to right) with strong rotation incident to a cape in the Southern Hemisphere: (a) $\hat{h} \approx 2.86$ and Ro ≈ 0.81; (b) $\hat{h} \approx 1.77$ and Ro ≈ 1.31. The masked areas depict the cape and other regions where measurements were not taken. Negative vertical velocity values indicate downward flow and are denoted by white dotted contours. The cross indicates the position of the vertical cross section shown in Fig. 3. The scale labeled L_R denotes the Rossby deformation radius.

$0.5h$ (giving $\alpha \approx 0.88$). For $z > z_d$ the upstream flow slows slightly as it approaches the obstacle and rises up the windward slope; that is, a flow-over regime dominates. Aloft of the cape the strong convergence accelerates the flow, which is consequently deflected to the left with a meridional velocity of around $0.4U_0$. The flow descends very sharply over the cape, following tightly to the leeward slope, and accelerates strongly toward the near surface. At the time of the experiment strong turbulent mixing was observed at the surface. A smooth mountain wave forms downstream with wavelength of around L_R. Accompanying the wave is strong deflection of the flow to the left with meridional velocity reaching $0.5U_0$. Downstream at $z > h$ the vectors become steeply sloping as if overturning is imminent. Here the zonal flow is much reduced and deflected to the right.

Figure 4b shows that at low level ($z \approx 0.4h$) the slowing and rising of the upstream flow is apparent over the entire length of the cape; that is, no stagnation point is evident (this is consistent with the dividing streamline height being approximately the measurement level $z \approx 0.4h$). Here the vertical velocity is $0–0.5U_0h/D$. The absence of lateral deflection upstream confirms that vertical deflection over the cape dominates. Downstream and parallel to the entire leeward slope is a band of strong descending flow with vertical velocity around $-3U_0h/D$, that is, approximately six times stronger than that upstream, consistent with Fig. 3b. Additionally, immediately against much of the leeward slope is a thin line of strong rising flow, consistent with strong turbulent mixing as the initial descending flow impacts on the surface. (This is not present in Fig. 3b as it begins to the "south" of the vertical cross section.) A lee jet develops downstream of the cape and is deflected to the left. This is strongest downstream of the middle and base sections of the cape, with velocities approaching three times that of the upstream flow. Centered on this jet and approximately a distance L_R downstream of the strong descending flow are regions where the vertical velocity reaches up to $2U_0$. The jet decays downstream over a distance of $\sim 2L_R$.

3) SENSITIVITY OF VERTICAL DEFLECTION TO NONDIMENSIONAL MOUNTAIN HEIGHT

Further investigation of the vertical deflection of flow over the cape and its sensitivity to $\hat{h}$ was achieved by comparing the mass flux incident upstream to the cape with the mass flux diverted laterally. In conjunction with the cape and bounding wall, a line upstream and perpendicular to the mean flow (shown as line B_y in Fig. 2) and a line from the tip of the cape intercepting line B_y (shown as line B_x) form a closed loop. Owing to the flow incompressibility, for $z < h$ the flux entering the loop across line B_y corresponds to the sum of the flux diverted horizontally and crossing line B_x and the

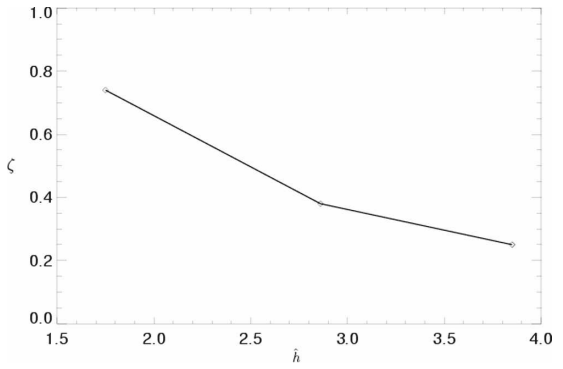

FIG. 5. Variation of ζ (the ratio of mass flux vertically deflected over the cape to incident mass flux) vs $\hat{h}$ for strong rotation. As ζ decreases the proportion of flow deflected vertically over the cape decreases. (Note an additional point, corresponding to $\hat{h} \approx 3.85$ and Ro ≈ 0.62, has been added. This represents a "very" blocked regime and is not discussed in the text.)

upward vertical flux through the horizontal surface inside the loop. We define η_x and η_y as the mass flux across lines B_x and B_y, and the ratio of mass flux vertically deflected over the cape to incident mass flux by the parameter ζ; that is,

$$\zeta = \sum_{z \approx 0.4h}^{z \approx h} \frac{\eta_y - \eta_x}{\eta_y}. \quad (1)$$

Figure 5 shows values of ζ against $\hat{h}$ for the blocked and flow-over regimes described above, showing that as $\hat{h}$ increases the proportion of flow deflected vertically over the cape decreases. An additional value of ζ corresponding to $\hat{h} \approx 3.85$ and Ro ≈ 0.62 has been added. However, as its flow response is similar to the "blocked" regime discussed above a fuller discussion of its flow regime has been omitted. As no measurements were included for near-surface levels, the values of ζ are more representative of small $\hat{h}$.

b. *Description of blocked and flow-over regimes under weak rotation*

To examine the sensitivity of the flow response to the Rossby number, an identical experiment was performed with a much slower rotation (i.e., a smaller value of f). Here the tank rotation rate was impulsively decreased from 999 to 338 s, giving $f = 0.037\ \text{s}^{-1}$ (i.e., around a third of the previous value) and $L_R \sim 160$ cm. Two flow fields were investigated with U_0 measured as 2.0 and 3.2 cm s^{-1}, giving similar values of $\hat{h}$ to those above of 3.00 and 1.88, respectively. Froude numbers are 0.17 and 0.28, and Rossby numbers are 2.70 and 4.32, respectively. The inversion height downstream of the cape tip was around $0.7h$ in both cases. Figures 6 and 7 (analogous to Figs. 3 and 4) present the normalized flow fields. Here $B/L_R \sim \frac{2}{3}$. Data are only available above the level $z \approx 0.5$–$0.6h$.

1) BLOCKED REGIME WITH WEAK ROTATION

Figure 6a shows the vertical cross section of the flow characterized by $\hat{h} \approx 3.00$ and Ro ≈ 2.70. Here $z_d \approx h$ (giving $\alpha \approx 0$); that is, all upstreamflow is blocked. The blocked flow is deflected to the left with a meridional velocity of around $0.1U_0$ and appears to extend farther upstream than shown (i.e., $\sim L_R$). Above the cape there is a small speed-up of the zonal wind with accompanying meridional deflection of $\sim 0.2U_0$, which descends a short distance down the lee slope. A weak lee wave is evident with a wavelength of around L_R. At upper levels (i.e., $z \approx 2h$) the zonal flow is only marginally affected by the cape.

Figure 7a shows that at midlevel ($z \approx 0.5$–$0.6h$) the upstreamflow divides in the horizontal plane when blocked, with negligible upward vertical movement. A stagnation point in the flow occurs at around $y \approx 0.6B$. To the right of this the flow is deflected along the side of the cape. To the left of this the flow is deflected toward the tip of the cape (consistent with Fig. 6a). As it passes around the tip it forms a detached jet approximately parallel to the x axis with a velocity around twice that of upstream. A weak, horizontally orientated, anticlockwise rotating eddy occurs to the cape's lee side.

2) FLOW-OVER REGIME WITH WEAK ROTATION

Figure 6b shows the vertical cross section of the flow incident to the cape characterized by $\hat{h} \approx 1.88$ and Ro ≈ 4.32. Here $z_d \approx 0.8h$ (giving $\alpha \approx 0.4$). For $z < z_d$ the flow slows as it approaches the cape. For $z > z_d$ it is deflected vertically over the cape. Aloft of the cape convergence accelerates the flow, which is deflected to the left with a velocity of around $0.2U_0$. The flow descends over the lee slope and accelerates strongly, though in the process becoming somewhat detached from the surface. Downstream the accelerated flow quickly decays.

Figure 7b shows that at midlevel ($z \approx 0.5$–$0.6h$) the slowing and rising of the upstream flow is apparent over the entire length of the cape. This is combined with broad horizontal deflection of the flow at either end of the cape. A stagnation point in the flow occurs at around $y \approx 0.6B$. Downstream of the cape and parallel to the entire leeward slope is a band of descending flow with vertical velocity approximately $-U_0 h/D$. Note that vertical deflection is strongest over the ends of the cape,

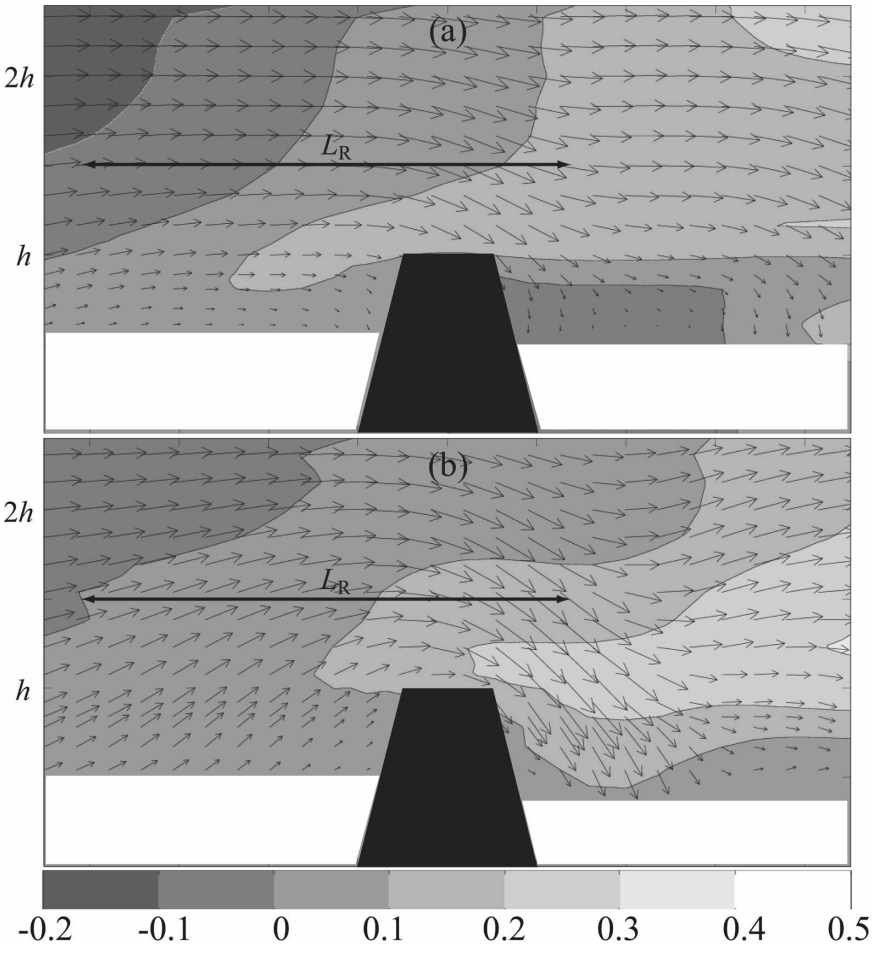

FIG. 6. As in Fig. 3 but with weak rotation: (a) $\hat{h} \approx 3.00$ and Ro ≈ 2.70 and (b) $\hat{h} \approx 1.88$ and Ro ≈ 4.32. Data are restricted to above the level 0.5–0.6h.

from where lee jets appear to develop. The lee wave that forms has a wavelength of approximately L_R.

3) EFFECT OF ROTATION ON THE SENSITIVITY OF VERTICAL DEFLECTION TO NONDIMENSIONAL MOUNTAIN HEIGHT

As the depth of flow sampled incident to the cape was smaller for the experiments with large Ro (i.e., Fig. 6) than for the experiments with small Ro (i.e., Fig. 3), direct comparison of values of ζ between experiments was not possible. Rather, Fig. 8 shows vertical profiles of $(\eta_y - \eta_x)/\eta_y$ (i.e., values are computed separately for each available vertical level), showing that for similar values of $\hat{h}$ the vertical deflection increases with strengthening rotation. Vertical deflection increases as the summit of the cape is approached. The result of Fig. 5 is confirmation that for similar Rossby number vertical deflection over the cape increases with decreasing $\hat{h}$.

4. Numerical mesoscale modeling of blocked and flow-over regimes

The flow response to the peninsula was investigated further by the numerical mesoscale modeling of two case studies representative of the blocked and flow-over regimes. Simulations were conducted using the Met Office Unified Model (UM) version 6.1 mesoscale model, with a horizontal resolution of 0.11° (approximately 12 km) and 38 vertical levels, using a "mesoscale" domain of 180 × 180 points centered over the peninsula (see Fig. 9). The model solves nonhydrostatic, deep-atmosphere dynamics using a semi-implicit, semi-Lagrangian numerical scheme (Cullen et al. 1997). It has a comprehensive set of parameterizations, including a scheme to represent drag due to gravity waves and low-level blocking from subgrid-scale orography (Webster et al. 2003). The model runs on a rotated latitude–longitude horizontal grid with Arakawa C staggering

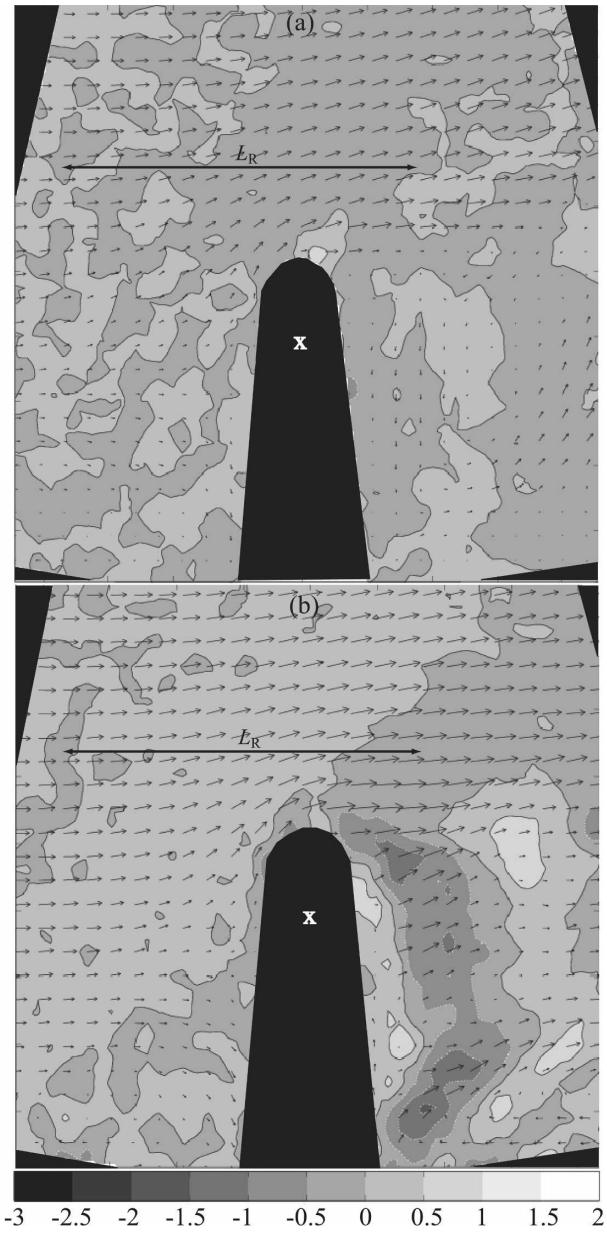

FIG. 7. As in Fig. 4 but with weak rotation and measured at a height $z \approx 0.5$–$0.6h$: (a) $\hat{h} \approx 3.00$ and Ro ≈ 2.70 and (b) $\hat{h} \approx 1.88$ and Ro ≈ 4.32.

and uses a terrain-following hybrid-height vertical coordinate with Charney-Philips staggering. The mesoscale model was one-way nested inside a global version with approximately 60-km resolution at this latitude and the same 38 vertical levels. ECMWF analysis data are used to initialize the model and included climatological sea ice fields.

Description of blocked and flow-over regimes

The case studies representing the blocked and flow-over regimes occurred at 0600 UTC 29 January 2002 and 0600 UTC 21 February 2002, respectively, that is, around the middle–end of the Southern Hemisphere summer. Figure 10 shows model horizontal and vertical wind speed at a height of 850 hPa for these times. Figures 11 and 12 show model zonal and meridional velocity and potential temperature along a vertical cross section extending around 2–3 L_R (~400 km) upstream and downstream of the peninsula and passing through the Faraday (i.e., at latitude 65.3°S or $y \approx 0.8B$ in the laboratory experiment coordinate frame) and over the northern section of the Larsen Ice Shelf (line C1 in Fig. 9). The climatological sea ice fields used for both case studies were similar, showing very little sea ice to the west of the northern peninsula, and over the eastern side very little at the far northern tip, increasing to a sea ice fraction of about 0.7 at 65°S. For each case the results are presented after the model has been integrated forward by 6 hours (i.e., from 0000 UTC).

Note that Fig. 9 shows that the model "resolved" orography is around 1000 m along the vertical cross section, significantly lower than the "actual" height of around 1500 m. However, a realistic estimate of the actual drag is found by combining the parameterized and resolved drag (Webster et al. 2003).

1) BLOCKED REGIME

On 29 January 2002 the ECMWF mean sea level pressure (MSLP) analysis for 0000 UTC showed a large low pressure (~970 hPa) system over the western Bellingshausen Sea. Consequently, early in the day well-defined westerly winds of moderate strength were incident to the peninsula. A weaker low pressure system (~980 hPa) existed northeast of the peninsula tip.

Figure 10a shows that at 0600 UTC the 850-hPa wind speed upstream of the northern section of the peninsula was around 5 m s^{-1}, giving $\hat{h} \approx 3.00$ ($=\hat{h}_{\mathrm{SAM}-}$), $F \approx 0.17$, and Ro ≈ 0.38 ($=\mathrm{Ro}_{\mathrm{SAM}-}$). As the flow approaches the peninsula, it is blocked. A stagnation point is evident at a latitude of around 66°S (i.e., south of Faraday, or equivalently $y \approx 0.7B$); that is, the flow is blocked. To the left (looking downwind) the flow turns toward the tip of the peninsula. Once past the tip it is rapidly deflected northward by the low pressure system to the northeast. To the right the flow is deflected in a southerly direction toward the base of the peninsula from where it is recirculated upwind. Further evidence that the flow travels around the peninsula, rather than over, is that with the exception of the northerly tip of the peninsula, the 850-hPa vertical velocity is negligible parallel to the western coast, and wind vectors are negligible over the peninsula itself. However, there is a thin line of weakly descending flow parallel to

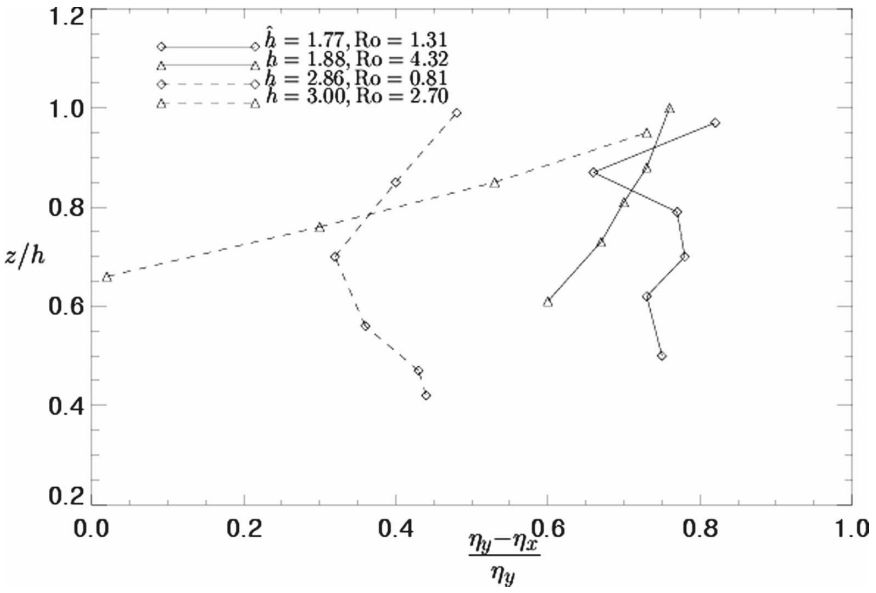

FIG. 8. Vertical profile of $(\eta_y - \eta_x)/\eta_y$ for strong and weak rotation.

much of the lee slope, which indicates that some vertical deflection occurs. An anticlockwise circulation is evident over the Weddell Sea. This is strongly influenced by katabatic winds blowing from the main Antarctic landmass.

The vertical cross section of Fig. 11a shows that for $z < h$ the upstream flow is blocked and unable to pass over the peninsula as Faraday is approached. Meridional flow is mostly weak (around 2 m s^{-1}) and southerly, consistent with Fig. 10a. A small region of weak northerly flow exists at near-surface level adjacent to the peninsula's western side, perhaps due to localized effects such as katabatic winds. Some descending flow is apparent over the lee slope at around summit level. Figure 11b shows isopycnals intersecting the upstream side of the peninsula. Here $z_d \approx 0.9h$ (giving $\alpha \approx 0.30$). To the lee of the peninsula a tightly packed layer of contours slightly below summit level also indicates that some flow is deflected over. This does not reach the near surface. Temperatures to the lee side of the peninsula are 2° to 4°C cooler than those upstream. Aloft of the peninsula the horizontal temperature gradient is small.

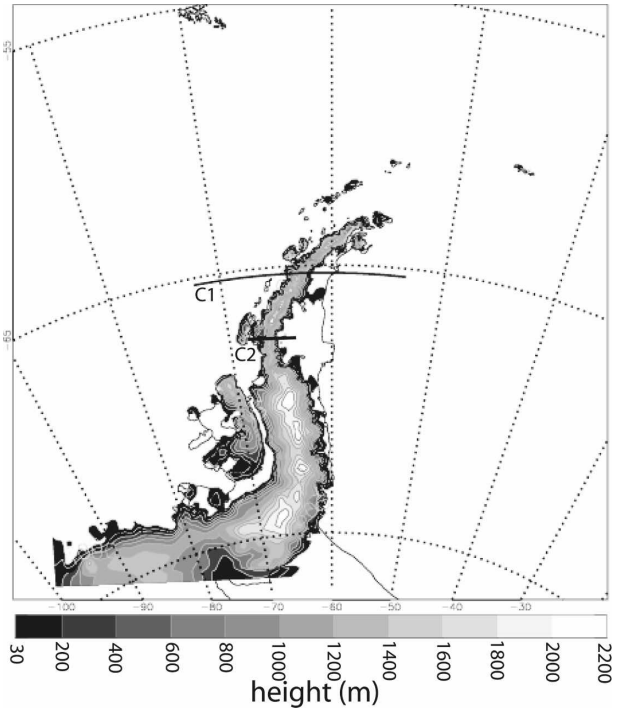

FIG. 9. Model Antarctic Peninsula orography height (m). The solid line labeled C1 indicates the position of the vertical cross section, passing through Faraday and over the northern section of the Larsen Ice Shelf (see Figs. 11 and 12). The solid line labeled C2 indicates the aircraft flight path, ascending from Rothera in the west (67.6°S, 68.1°W) to an altitude of 3000 m, before flying eastward over the peninsula and descending over the Larsen Ice Shelf (see Fig. 14).

2) FLOW-OVER REGIME

On 21 February 2002 the ECMWF MSLP analysis for 0000 UTC showed large, deep low pressure systems over the Bellingshausen Sea (~965 hPa) and the Weddell Sea (~970 hPa). Situated to the northwest of the peninsula was a strong high pressure system. Consequently, early in the day the isobars were situated close

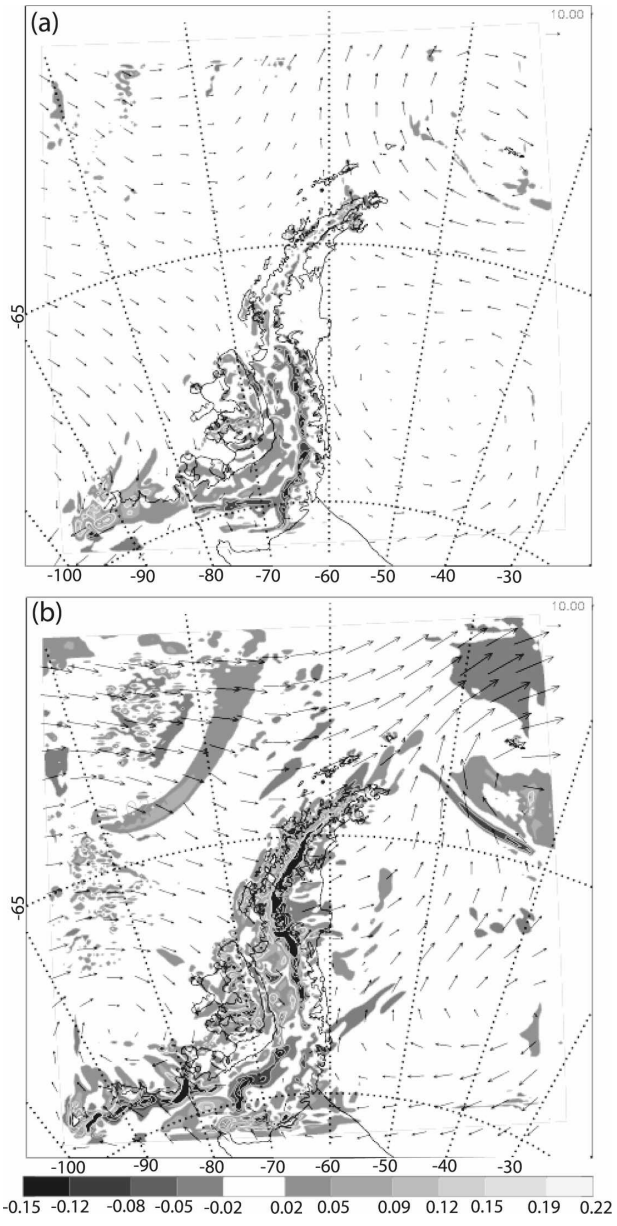

FIG. 10. Horizontal (vectors) and vertical (shading) velocity (m s^{-1}) over the Antarctic Peninsula at the 850-hPa level showing (a) blocked conditions (0600 UTC 29 Jan 2002) and (b) flow-over conditions (0600 UTC 21 Feb 2002): (a) $\hat{h} \approx 3.00$ and Ro ≈ 0.38 and (b) $\hat{h} \approx 1.50$ and Ro ≈ 0.76. Computed using a 6-h integration of UM 6.1 with a horizontal resolution of 12 km. Vectors are shown every eight grid points.

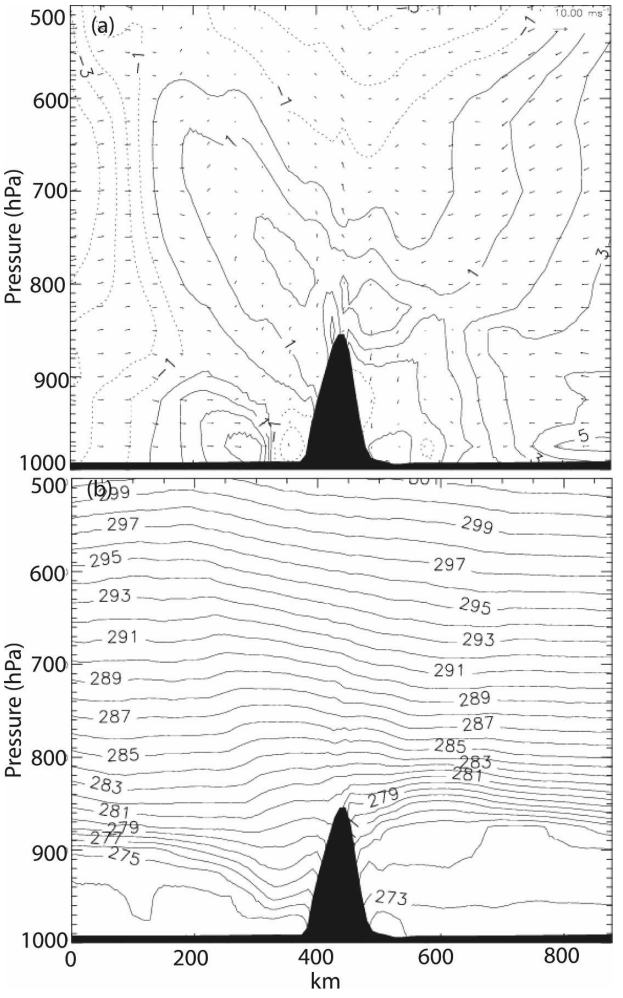

FIG. 11. Vertical cross section for blocked conditions, showing (a) zonal (vectors; interpolated onto evenly spaced pressure levels) and meridional (contours) velocity (m s^{-1}) and (b) potential temperature (K) in a vertical cross section perpendicular to the Antarctic Peninsula, passing through Faraday and over the northern section of the Larsen Ice Shelf (line C1 in Fig. 9) (i.e., 65.3°S or $y \approx 0.8B$ in the laboratory experiment coordinate frame) for 0600 UTC 29 Jan 2002. Here $\hat{h} \approx 3.00$ and Ro ≈ 0.38. Computed using a 6-h integration of UM 6.1 with a horizontal resolution of 12 km. Negative meridional values are displayed by dashed contours.

to each other and the peninsula was under the influence of well-defined, strong westerly winds.

Figure 10b shows that at 0600 UTC the 850-hPa wind speed upstream of the northern section of the peninsula was around 10 m s^{-1}, giving $\hat{h} \approx 1.50$ (i.e., smaller than $\hat{h}_{\mathrm{SAM+}}$ and greater than $\hat{h}_{\mathrm{strong}}$), $F \approx 0.35$, and Ro $\approx$ 0.76 (i.e., representative of $\mathrm{Ro}_{\mathrm{SAM+}}$). Westerly winds pass over the northern and middle sections of the peninsula (i.e., any stagnation point is below 850 hPa) but remain blocked over the much higher orography to the south. This is confirmed by the 850-hPa vertical velocity field showing rising flow (>0.05 m s^{-1}) immediately upstream of the entire length of the peninsula. The flow that is able to pass over the peninsula accelerates and descends strongly down the lee slope. Here the vertical velocity increases by a factor of 3 (~ -0.15 m s^{-1}). Downstream the flow is deflected to the left by the low pressure system over the Weddell Sea.

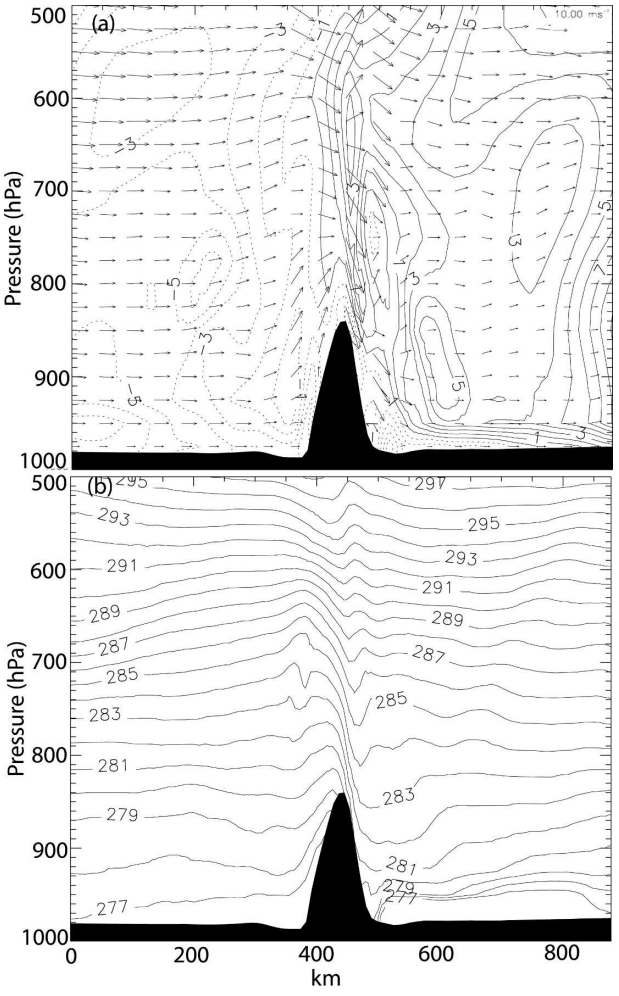

FIG. 12. As in Fig. 11 but for flow-over conditions for 0600 UTC 21 Feb 2002: $\hat{h} \approx 1.50$ and Ro ≈ 0.76.

The vertical cross section of Fig. 12a shows $z_d \approx 0.5h$ (giving $\alpha \approx 0.75$). For $z_d < z < h$ the upstream flow is deflected over the northern section of the peninsula. Strong acceleration occurs throughout a thick layer aloft of the peninsula (the velocity reaching around 20 m s^{-1}). Here the meridional velocity is southerly. The flow descends as it passes over the peninsula, following very closely to the leeward slope as it accelerates strongly toward the near surface. Downslope winds are approximately three times as strong as their upstream value and decay over a distance of 1–2 L_R (i.e., 150–300 km). Downstream meridional winds are southerly.

Figure 12b shows isopycnals rising up the upstream side of the peninsula and intersecting at heights $>0.5h$, confirming the estimate of z_d. It is further confirmed that the descending flow is significantly stronger than the ascending upstream flow and reaches close to the near surface of the lee side. This brings warm upper-level air down to the lee side, giving rise to a temperature difference of up to 3°C between the lee side and upstream.

5. Discussion and conclusions

Marshall et al. (2006) demonstrated that the stronger summer westerlies, associated with the recent positive trend in the SAM, are driving rising near-surface temperatures in the northeast Antarctic Peninsula. Over the past 40 years summer temperatures have increased here by more than 2°C (making it one of the most rapidly warming regions on the surface of the earth), three times that observed on the northwest side. This has undoubtedly played a major role in the break up of northern sections of the Larsen Ice Shelf. The mechanism proposed for this warming is not so much that the westerlies are blocked by the peninsula (a mechanism that has maintained the markedly different climates between the east and west sides), as that the strengthening winds increase the transport of relatively warm, maritime air masses over the peninsula. These air masses warm further adiabatically as they descend down the easterly leeward slope. Moreover, an additional contribution to the warming comes from the weaker easterlies, which are associated with the stronger westerlies (see Fig. 8 of Marshall et al. 2006).

Here we examined this mechanism by studying the flow characteristics of the peninsula through a laboratory model of simple idealized flow incident to a cape (and in particular over its northern section), using a large value of the Coriolis parameter to simulate the influence of the peninsula's high-latitude location. Two distinct flow regimes were identified that were dependent on the nondimensional mountain height; a "blocked" regime ($\hat{h} \approx 2.86$; Ro ≈ 0.81; $F \approx 0.18$; $z_d \approx 0.7h$; $\alpha \approx 0.86$) characterized by almost all upstream flow passing around the peninsula, and a "flow-over" regime ($\hat{h} \approx 1.77$; Ro ≈ 1.31; $F \approx 0.30$; $z_d \approx 0.5h$; $\alpha \approx 0.88$) characterized by considerable vertical deflection of the upstream flow over the peninsula and strong downslope winds reaching near-surface level to the lee. Upper-air observations from Bellingshausen showed the value of $\hat{h}$ characteristic of the northern tip of the peninsula has decreased from around 2.14 to 1.20 over the period from 1965 to 1997. Based on the laboratory model this corresponds to a change from a blocked to a flow-over regime, that is, a transition from a regime where blocked conditions dominate to one where the frequency of occurrence of flow-over conditions increases with consequent warming implications.

Additional numerical experiments of selected cases at a high resolution of 12 km were used to further un-

derstand the flow response: a blocked regime ($\hat{h} \approx 3.00$; Ro ≈ 0.38; $F \approx 0.16$; $z_d \approx 0.9h$; $\alpha \approx 0.30$) and a flow-over regime ($\hat{h} \approx 1.50$; Ro ≈ 0.76; $F \approx 0.31$; $z_d \approx 0.5h$; $\alpha \approx 0.75$). These suggested that, for the same value of $\hat{h}$ and similar low Rossby number, the numerical simulated flow response deflects less flow over the peninsula as compared to the laboratory simulation. However, both simulations of the flow-over regime agree that the downslope winds are considerably stronger than the upslope winds and reach the near-surface of the lee side. Both simulations of the blocked regime give the same location of the stagnation point as $y \approx 0.7B$.

In terms of the temperature response, the flow-over case study confirmed considerable leeside warming. However, it is noticeable that the strong downslope wind slows markedly as it approaches the near surface and that here the warming effect is small (Fig. 12b). Most likely this is due to the large climatological sea ice fraction (around 0.7) used by the model in this region, implying that the atmosphere is comparatively strongly stratified and that penetration of the warm downslope wind is restricted. The actual sea ice coverage for this case study (not shown) was negligible over the eastern northern peninsula, which is perhaps more typical for the middle–end of the Southern Hemisphere summer. Under these circumstances the downslope wind and its resulting warming might be expected to reach the surface, suggesting that accurate surface forcing plays an important role in being able to reproduce this correctly.

Over the northern section of the peninsula the climatology based on ERA-40 analysis showed for SAM− ($\hat{h}_{\mathrm{SAM-}} \sim 3.00$) a blocked regime dominated, while for SAM+ ($\hat{h}_{\mathrm{SAM+}} \sim 1.88$) a flow-over regime dominated, indicating a broadly similar flow response and sensitivity to $\hat{h}$ as the results described here. These values of $\hat{h}$ are perhaps more representative of the northern section of the peninsula rather than the lower values determined by the strong winds measured at Bellingshausen, verifying again the proposed warming mechanism. Close comparison with the high-resolution numerical simulation, which more accurately modeled the peninsula height, does suggest, however, that the ERA-40 SAM+ climatology underestimates the amount of flow deflected over the peninsula and limits it too far to the north. It should be stressed that the ERA-40 horizontal resolution of ~125 km severely underestimates the peninsula height, and thus the simulated atmospheric flow relies heavily on the subgrid-scale parameterization of low-level blocking and gravity wave breaking (Lott and Miller 1997). Nevertheless, this conclusion is consistent with the results of Van Lipzig et al. (2008) who used a regional atmospheric model to develop a "high resolution" climatology (horizontal resolution of 14 km) of summers with positive and negative SAM indexes, which compared to ERA-40 showed the region of flow-over and associated leeside warming in response to SAM+ extending farther to the south and reaching the northern section of the Larsen Ice Shelf. This suggests that there is the possibility that weather systems that pass over the peninsula are in reality being prevented from doing so in the ERA-40 reanalysis. This is supported by Fig. 13, which shows a comparison between radiosonde and ERA-40 mean summer wind profiles, indicating that at heights aloft of the peninsula both the zonal and meridional modeled components of the flow are too strong downstream of its northern tip (at Marambio); that is, the flow is excessively blocked upstream of the peninsula's northern section and directed around and consequently over the tip's comparatively low orography (see Fig. 9). Upstream of the peninsula (at Bellingshausen) the ERA-40 and sonde values are in excellent agreement (cf. Fig. 13).

Moreover, this study had demonstrated the important impact that the strong Coriolis force has on the flow characteristics of the peninsula. Laboratory experiments with weak rotation showed that for both large ($\hat{h} \approx 3.00$; Ro ≈ 2.70; $F \approx 0.17$; $z_d \approx H$; $\alpha \approx 0$) and small ($\hat{h} \approx 1.88$; Ro ≈ 4.32; $F \approx 0.28$; $z_d \approx 0.8H$; $\alpha \approx 0.4$) values of $\hat{h}$, considerably less fluid was deflected over the cape than for flows with strong rotation. Consequently, the downslope wind strength was considerably increased under strong rotation. Furthermore, it was noticed that with weak rotation the downslope wind was rather detached from the lee slope.

For both regimes the experiment with strong rotation showed considerable deflection to the left of flow downstream of the right hand side of the cape, as Baines and Fraedrich (1989) showed, consistent with the flow being particularly deflected over this side (as discussed in section 2). The abutting wall prevents any flow from traveling around the right hand side of the cape, enhancing further the flow asymmetry. Thus a considerable amount of flow is able to pass over the middle and southern sections of the peninsula (see Fig. 10b), despite the comparatively high orography (~2000 m) and weak upstream zonal wind (see Fig. 6 of Marshall et al. 2006), that is, large $\hat{h}$. This is supported by Fig. 14, which compares upstream and downstream vertical profiles of potential temperature and relative humidity measured on 6 January 2006 by an aircraft flying over the middle section of the peninsula from Rothera in the west (67.6°S, 68.1°W) to the Larsen Ice Shelf in the east (line C2 in Fig. 9; J. C. King et al. 2007, unpublished manuscript). A radiosonde launched at Rothera a few hours before the flight gave a wind speed

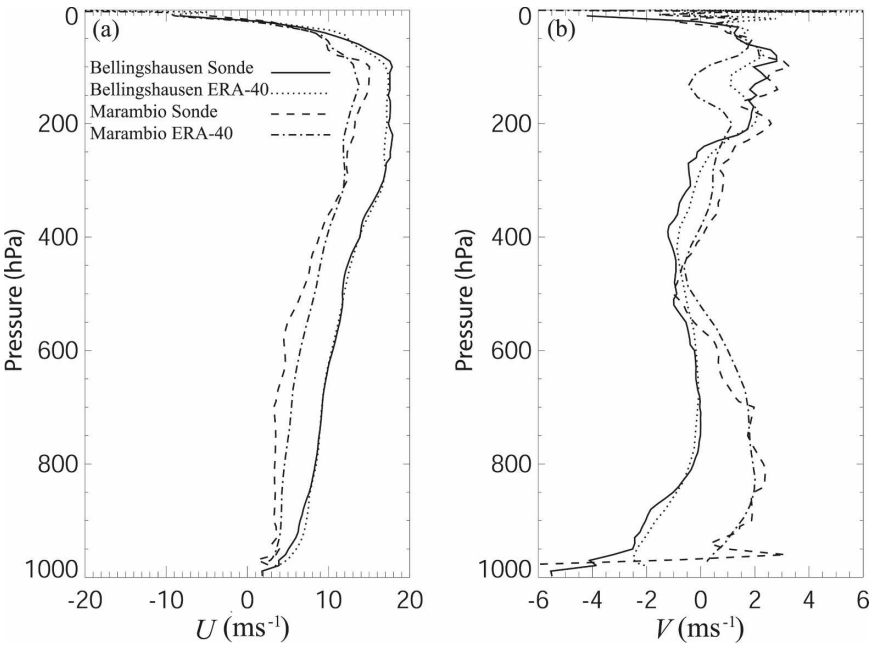

FIG. 13. Comparison of ERA-40 and radiosonde mean (a) zonal and (b) meridional wind profiles (24 cases over the period 1 Dec 1998 to 31 Jan 1999) for Bellingshausen (at 0000 UTC) and Marambio (at 1200 UTC).

of 5 m s^{-1} at a height of around 1000 m, giving $\hat{h} \approx 4$. Despite this large value of $\hat{h}$, the figure shows that air downstream of the peninsula is significantly warmer and drier than that upstream, indicating that considerable flow-over is occurring. This suggests that the region of the peninsula where the flow regime is strongly influenced by the strengthening westerlies extends considerably to the south (as suggested by Van Lipzig et al.

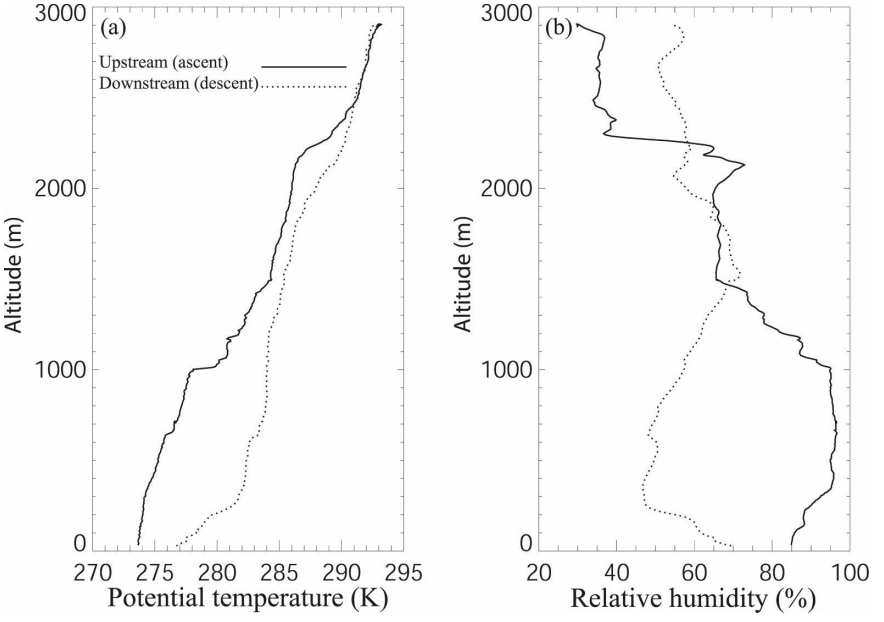

FIG. 14. Vertical profiles of (a) potential temperature (K) and (b) relative humidity (%) measured upstream (solid line) and downstream (dotted line) on 6 Jan 2006 by an aircraft ascending from Rothera in the west (67.6°S, 68.1°W) to an altitude of 3000 m before flying eastward over the peninsula and descending over the Larsen Ice Shelf (line C2 in Fig. 9).

2008), with the associated leeside warming threatening further extensive stretches of the Larsen Ice Shelf.

Finally, the proposed warming mechanism is probably relevant to other mountainous areas outside Antarctica. For example, Prömmel et al. (2007) showed a strong correlation between the positive North Atlantic Oscillation (NAO) (bringing stronger westerly flow over middle and northern Europe) and warm winter temperatures to the lee of the Alps.

Acknowledgments. The authors are grateful to the two anonymous reviewers, whose comments and suggestions improved the manuscript. We thank T. Lachlan-Cope for making the aircraft measurements shown in Fig. 14. Thanks to ECMWF for allowing access to their ERA-40 data. This work was supported by grants from NERC to the Centre for Polar Observation and Modelling, University College London. The laboratory work was supported by EEC Contract "Transnational Access to Major Research Infrastructures," HPRI CT 20000168, with much technical support from S. Decamp, H. Didelle, S. Mercier, E. Thivolle-Cazat, and S. Viboud. Thanks also to S. Farrell, A. Muir, and P. Taylor for help producing the figures, J.-F. Gueganton for computer support, and P. Baines and A. Beljaars for useful conversation.

REFERENCES

Baines, P. G., 1979: Observations of stratified flow past three-dimensional barriers. *J. Geophys. Res.,* **84,** 7834–7838.

——, 1995: *Topographic Effects in Stratified Flows*. Cambridge University Press, 482 pp.

——, and K. P. Hoinka, 1985: Stratified flow over two-dimensional topography in fluid of infinite depth: A laboratory simulation. *J. Atmos. Sci.,* **42,** 1614–1630.

——, and K. Fraedrich, 1989: Topographic effects of the mean tropospheric flow patterns around Antarctica. *J. Atmos. Sci.,* **46,** 3401–3416.

——, and R. B. Smith, 1993: Upstream stagnation points in stratified flow past obstacles. *Dyn. Atmos. Oceans,* **18,** 105–113.

Beran, D. W., 1967: Large amplitude lee waves and chinook winds. *J. Appl. Meteor.,* **6,** 865–877.

Boyer, D. L., and R.-R. Chen, 1987: Laboratory simulation of mountain effects on large-scale atmospheric motion systems: The Rocky Mountains. *J. Atmos. Sci.,* **44,** 100–123.

——, and P. A. Davies, 2000: Laboratory studies of orographic effects in rotating and stratified flows. *Ann. Rev. Fluid Mech.,* **32,** 165–202.

Cullen, M. J. P., T. Davies, M. H. Mawson, J. A. James, S. C. Coulter, and A. Malcolm, 1997: An overview of numerical methods for the next generation U.K. NWP and climate model. *Numerical Methods in Atmospheric and Ocean Modeling: The André J. Robert Memorial Volume,* C. A. Lin et al., Eds., NRC Research Press, 425–444.

Ding, L., and R. L. Street, 2003: Numerical study of the wake structure behind a three-dimensional hill. *J. Atmos. Sci.,* **60,** 1678–1690.

Fincham, A., and G. Delerce, 2000: Advanced optimization correlation imaging velocimetry algorithms. *Exp. Fluids,* **29,** 13–22.

Georgelin, M., and E. Richard, 1996: Numerical simulation of flow diversion around the Pyrenees: A tramontana case study. *Mon. Wea. Rev.,* **124,** 687–700.

Hunt, J. C. R., and W. H. Snyder, 1980: Experiments on stably and neutrally stratified flow over a model three dimensional hill. *J. Fluid Mech.,* **96,** 671–704.

——, Y. Feng, P. F. Linden, M. D. Greenslade, and S. D. Mobbs, 1997: Low Froude number stable flows past mountains. *Il Nuovo Cimento,* **20C,** 261–271.

——, H. Ólafsson, and P. Bougeault, 2001: Coriolis effects on orographic and mesoscale flows. *Quart. J. Roy. Meteor. Soc.,* **127,** 601–633.

King, J. C., 1994: Recent climate variability in the vicinity of the Antarctic Peninsula. *Int. J. Climatol.,* **14,** 357–369.

——, and J. Turner, 1997: *Antarctic Meteorology and Climatology*. Cambridge University Press, 409 pp.

——, and S. A. Harangozo, 1998: Climate change in the western Antarctic Peninsula since 1945: Observations and possible causes. *Ann. Glaciol.,* **27,** 571–575.

——, J. Turner, G. J. Marshall, W. M. Connolley, and T. A. Lachlan-Cope, 2003: Antarctic Peninsula climate variability and its causes as revealed by instrumental records. *Antarctic Peninsula Climate Variability: Historical and Paleoenvironmental Perspectives,* E. Domack et al., Eds., Antarctic Research Series, Vol. 79, Amer. Geophys. Union, 17–30.

Kwok, R., and J. Comiso, 2002: Spatial patterns of variability in Antarctic surface temperature: Connections to the Southern Hemisphere annular mode and the Southern Oscillation. *Geophys. Res. Lett.,* **29,** 1705, doi:10.1029/2002GL015415.

Lilly, D. K., 1978: A severe downslope windstorm and aircraft turbulence event induced by a mountain wave. *J. Atmos. Sci.,* **35,** 59–77.

Lott, F., and M. J. Miller, 1997: A new subgrid-scale orographic drag parameterization: Its formulation and testing. *Quart. J. Roy. Meteor. Soc.,* **123,** 101–127.

Marshall, G. J., 2002: Analysis of recent circulation and thermal advection change in the northern Antarctic Peninsula. *Int. J. Climatol.,* **22,** 1557–1567.

——, 2003: Trends in the Southern Annular Mode from observations and reanalyses. *J. Climate,* **16,** 4134–4143.

——, P. A. Stott, J. Turner, W. M. Connolley, J. C. King, and T. A. Lachlan-Cope, 2004: Causes of exceptional circulation changes in the Southern Hemisphere. *Geophys. Res. Lett.,* **31,** L14205, doi:10.1029/2004GL019952.

——, A. Orr, N. P. M. Van Lipzig, and J. C. King, 2006: The impact of a changing Southern Hemisphere annular mode on Antarctic Peninsula summer temperatures. *J. Climate,* **19,** 5388–5404.

Ólafsson, H., 2000: The impact of flow regimes on asymmetry of orographic drag at moderate and low Rossby numbers. *Tellus,* **52A,** 365–379.

——, and P. Bougeault, 1996: Nonlinear flow past an elliptic mountain ridge. *J. Atmos. Sci.,* **53,** 2465–2489.

——, and ——, 1997: The effect of rotation and surface friction on orographic drag. *J. Atmos. Sci.,* **54,** 193–210.

Orr, A., D. Cresswell, G. J. Marshall, J. C. R. Hunt, J. Sommeria, C. G. Wang, and M. Light, 2004: A "low-level" explanation for the recent large warming trend over the western Antarctic Peninsula involving blocked winds and changes in zonal cir-

culation. *Geophys. Res. Lett.,* **31,** L06204, doi:10.1029/2003GL019160.

——, E. Hanna, J. C. R. Hunt, J. Cappelen, K. Steffen, and A. Stephens, 2005: Characteristics of stable flows over southern Greenland. *Pure Appl. Geophys.,* **162,** 1747–1778.

Pierrehumbert, R. T., and B. Wyman, 1985: Upstream effects of mesoscale mountains. *J. Atmos. Sci.,* **42,** 977–1003.

Prömmel, K., M. Widmann, and J. M. Jones, 2007: Analysis of the (N)AO influence on alpine temperatures using a dense station dataset and a high-resolution simuluation *Geophysical Research Abstracts,* Vol. 9, Abstract 06165. [Available online at http://www.cosis.net/abstracts/EGU2007/06165/EGU2007-J-06165.pdf?PHPSESSID=e.]

Smith, R. B., 1989: Hydrostatic airflow over mountains. *Advances in Geophysics,* Vol. 31, Academic Press, 1–39.

——, and S. Grønås, 1993: Stagnation points and bifurcation in 3-D mountain airflow. *Tellus,* **45A,** 28–43.

Thompson, D. W. J., and S. Solomon, 2002: Interpretation of recent Southern Hemisphere climate change. *Science,* **296,** 895–899.

——, J. M. Wallace, and G. C. Hegerl, 2000: Annular modes in the extratropical circulation. Part II: Trends. *J. Climate,* **13,** 1018–1036.

Van den Broeke, M. R., and N. P. M. Van Lipzig, 2003: Response of wintertime Antarctic temperatures to the Antarctic Oscillation: Results of a regional climate model. *Antarctic Peninsula Climate Variability: Historical and Paleoenvironmental Perspectives,* E. Domack et al., Eds., Antarctic Research Series, Vol. 79, Amer. Geophys. Union, 43–58.

Van Lipzig, N. P. M., G. J. Marshall, A. Orr, and J. C. King, 2008: The relationship between the Southern Hemisphere annular mode and Antarctic Peninsula summer temperatures: Analysis of a high-resolution model Climatology. *J. Climate,* **21,** 1649–1668.

Vaughan, D. G., G. J. Marshall, W. M. Connolley, J. C. King, and R. Mulvaney, 2001: Climate change: Devil in the detail. *Science,* **293,** 1777–1779.

——, and Coauthors, 2003: Recent rapid regional climate warming on the Antarctic Peninsula. *Climatic Change,* **60,** 243–274.

Vosper, S. B., I. P. Castro, W. H. Snyder, and S. D. Mobbs, 1999: Experimental studies of strongly stratified flow past three-dimensional orography. *J. Fluid Mech.,* **390,** 223–249.

Webster, S., A. R. Brown, D. R. Cameron, and C. P. Jones, 2003: Improvements to the representation of orography in the Met Office Unified Model. *Quart. J. Roy. Meteor. Soc.,* **129,** 1989–2010.